

## Design of Novel Nanoparticles for Thin-film Solar Cells

Shiwei Zhou<sup>1</sup>, Qing Li<sup>2</sup>, Scott Townsend<sup>2</sup>, Yi Min Xie<sup>1</sup>, Xiaodong Huang<sup>1</sup>

<sup>1</sup> Centre for Innovative Structures and Materials, School of Civil, Environmental and Chemical Engineering, RMIT University, GPO Box 2476, Melbourne 3001, Australia, [shiwei.zhou, mike.xie, xiaodong.huang@rmit.edu.au](mailto:shiwei.zhou, mike.xie, xiaodong.huang@rmit.edu.au),

<sup>2</sup> School of Aerospace, Mechanical and Mechatronics Engineering, The University of Sydney, Sydney, NSW 2006, Australia, [qing.li, scott.townsend@sydney.edu.au](mailto:qing.li, scott.townsend@sydney.edu.au)

### 1. Abstract

We use Gielis' superformula with a small number of parameters to define a wide variety of 3D geometries ranging from common shapes like sphere, cube, octahedron and cylinder to highly complex structures. This allows us to search for the optimal shape of nanoparticles embedded in the rear dielectric layer of thin-film solar cells by employing an evolutionary algorithm to maximize the short circuit current density. By using this optimization technique, we have found a lens-like nanoparticle capable of improving the short circuit current density to 19.11 mA/cm<sup>2</sup>. Compared with an advanced two-scale nanospherical configuration that was recently reported to synthesize the merits of large and small spheres into a single structure, our new design has achieved a further 3.3% improvement in the short circuit current density. In addition, the novel nanoparticle we have obtained is much more fabrication-friendly due to its simple shape and tolerance to geometrical distortions. As alternatives, novel starfish-like nanomorphologies with four, six or eight arms are also found from the optimization to have large short circuit current density.

**2. Keywords:** Thin-film solar cell, nanoparticle, light trapping, evolutionary algorithm, shape optimization.

### 3. Introduction

The request for 'optically thick' photovoltaic absorbers to attain maximal light absorption and photo carrier current collection in thin-film solar cell can be fulfilled by using some light trapping techniques [1]. For example, the metallic nanoparticles built in the solar cells can trigger localized surface plasmon through which the incident light is scattered by the nanoparticles at larger angles with drastically electric enhanced intensity when propagating into the absorber layer. As a result, the effective light path in a thin absorber layer can be prolonged to a level equivalent or superior to the conventional wafer-based solar cells. Proposals of such thin-film solar cells [2] have drawn increasing attention as they reduce the consumption of semiconductor materials and can be easily fabricated in mass-production.

The light trapping mechanism is however very sensitive to the geometrical configuration of the nanoparticles. In addition to various randomly-shaped structures [3, 4], the effects of some primitive geometries such as cylinder, sphere and hemisphere on light trapping have been investigated [3-6]. It was reported that the cylindrical and hemispherical particles have better performance than spherical particles [4]. The nanoparticle size is another critical parameter in light trapping. The merits of nanoparticles in different length scales can coexist when they are synthesized into a single structure. A prominent example is a larger sphere evenly covered by half-truncated small spheres on its surface, in which the large and small spheres serve as light-intensity-amplifier and lighter-angle-refractor, respectively [7]. In a properly sized configuration, this novel nanostructure results in a large short circuit current density ( $J_{sc}$ ) as well as a high conversion efficiency.

While the abovementioned seminal works have established a basic relationship between light trapping effect and the size of nanoparticles, where smaller ones scatter more light in the absorber [4] and larger ones have less Ohmic loss, the study on the role of the nanoparticle shape in light trapping for thin-film solar cells remains rather limited. One of the reasons why this issue has received less attention to date resides in the major difficulties of numerically modelling various 3D complex shapes. Fortunately, the recently-developed Gielis superformula [8] offers a simple formulation for defining a broad range of sophisticated shapes using only a small number of geometrical parameters. In view of its recent success in studying the geometry for soft porous system (i.e. adaptive structure undergoing large shape change) [9] and plasmonic nanowires [10] in 2D, it appears promising to explore this superformula in 3D space for searching the optimal nanoparticle in thin-film solar cells.

### 3. Methodology

As shown in Figure 1a, the structure of a thin-film solar cell studied in this paper consists of four ordered layers: a 80 nm SnO<sub>2</sub>:F coated in glass as a transparent conductive oxide on the front; followed by a 350 nm hydrogenated amorphous silicon (a-Si:H) layer; subsequently a layer of Al-doped ZnO (ZnO:Al) thin-film embedded with periodic Ag particles; and finally a 120 nm Ag back reflector. The configuration of such a layered structure comes

from the studies on two-scale nanospheres (Figure 1b), which is desirable for thin-film solar cells as the merits of large sphere (strong resonant intensity of field) and small spheres (large scattering angles) coexist in this nanostructure [7]. To ensure an optimal nanoparticle coverage (10%), the distance between two nanoparticles is 792.67 nm. Numerical study showed that the solar cell reaches the largest  $J_{sc}$  when the radii of small and larger spheres are 20 nm and 100 nm [7]. As the solar cell embedded with such two-scale nanospheres has been employed as a benchmark, all the nanoparticles studied thereafter are given the same size and periodicity for a fair comparison.

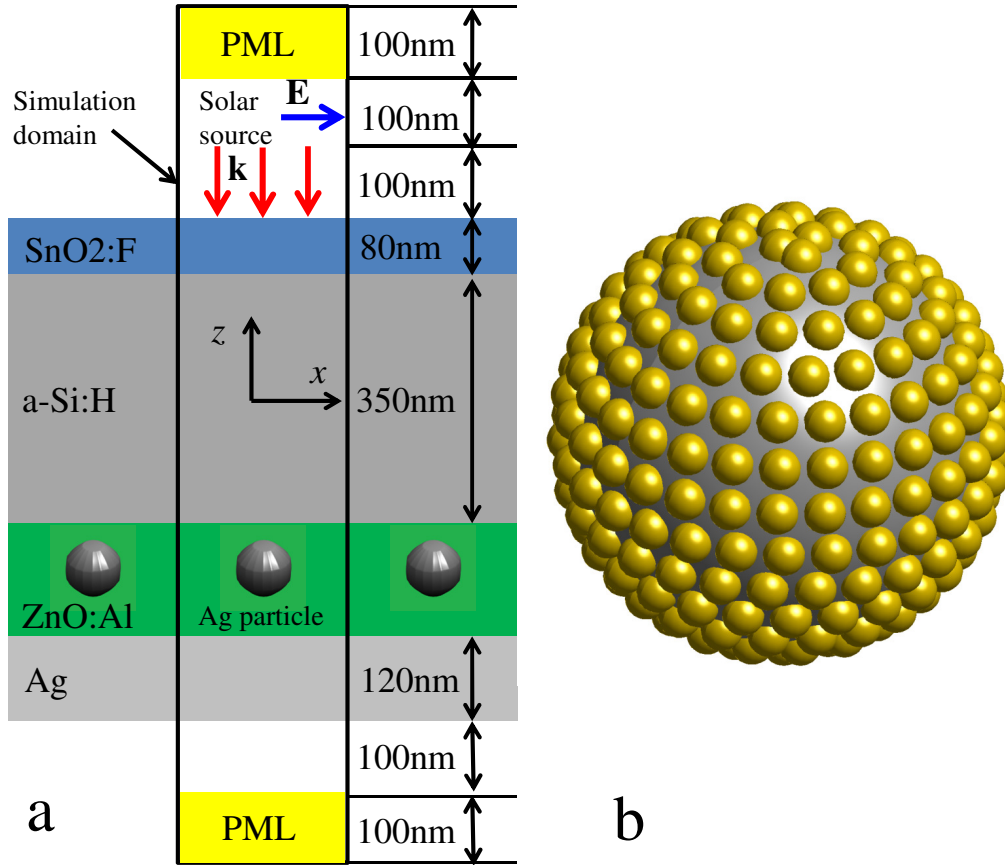


Figure 1: (a) Schematic of the thin-film solar cell with silver nanoparticles; (b) 3D view of the two-scale nanosphere

Since the nanospheres are periodically-placed and the incident light is normal to the front surface (the directions of wave vector  $\mathbf{k}$  and electric field  $\mathbf{E}$  are indicated by the red and blue arrows respectively in Figure 1a), it is sufficient to restrain the modeling region to a representative volume element (RVE, the black rectangle in Figure 1a) with periodic boundary conditions applied to its bilateral faces. The open boundaries on the input and output sides are truncated by Perfectly Matched Layers (PMLs, the yellow regions in Figure 1a), whose distances to the top and bottom of solar cell are 200 nm and 100 nm, respectively. In the RVE, the solar source is placed on a plane whose distance to the SnO<sub>2</sub>:F layer is 100 nm.

The electromagnetic field within the RVE is governed by Maxwell's equations and solved by the finite difference time domain (FDTD) algorithm [11]. In the present study, we utilize the FDTD program from Lumerical as it has been used by many researchers in this area [12]. By taking advantage of the symmetry and anti-symmetry at the  $x$  and  $y$  directions, the computational domain can be reduced to a quarter of the base cell without violating its periodicity.

In a spherical coordinate, the position of any surface point can be calculated as  $x=r(\theta)\cos(\theta) r(\varphi)\cos(\varphi)$ ,  $y=r(\theta)\sin(\theta)r(\varphi)\cos(\varphi)$  and  $z=r(\theta)\sin(\varphi)$ , where the ranges of azimuthal and polar angles are  $-\pi \leq \theta \leq \pi$  and  $-\pi/2 \leq \varphi \leq \pi/2$ , respectively. The radius of Gielis shape is defined by:

$$r(\theta) = \left( \left| \cos(m\theta/4)/a \right|^{p_2} + \left| \sin(m\theta/4)/b \right|^{p_2} \right)^{-1/n_1} \quad (1)$$

The scale of the 3D object is determined by factors  $a$  and  $b$  while its shape is controlled by shape coefficients  $n_1$ ,  $n_2$  and  $n_3$ . The number of rotational symmetries is governed by parameter  $m$ , which indicates the number of vertices in the  $x$ - $y$  cross-section. To increase the shape variety, two sets of parameters, namely  $(m, n_1, n_2, n_3)$  and  $(q, n_4, n_5, n_6)$ , are employed to generate  $r(\varphi)$  and  $r(\theta)$ , respectively. For the nanostructure considered in the thin-film solar cell, its shape is generally square-symmetry in the plane normal to the incident wave (e.g.  $x$ - $y$  plane), thus  $m$  and  $q$  must be remained an even number in the design. To decrease the design parameters,  $n_2=n_3$  and  $n_5=n_6$  are imposed without influencing the diversity of Gielis shapes. Following abovementioned prerequisites, Figure 2 illustrates a class of nanostructures derived from the Gielis' superformula. It is noted that in addition to such common geometries as sphere, cube, octahedron and cylinder which have been well studied, there are many novel structures, including a remarkable structure in column 3 and row 3 in Figure 2, which resembles the two-scale nanosphere in Figure 1b.

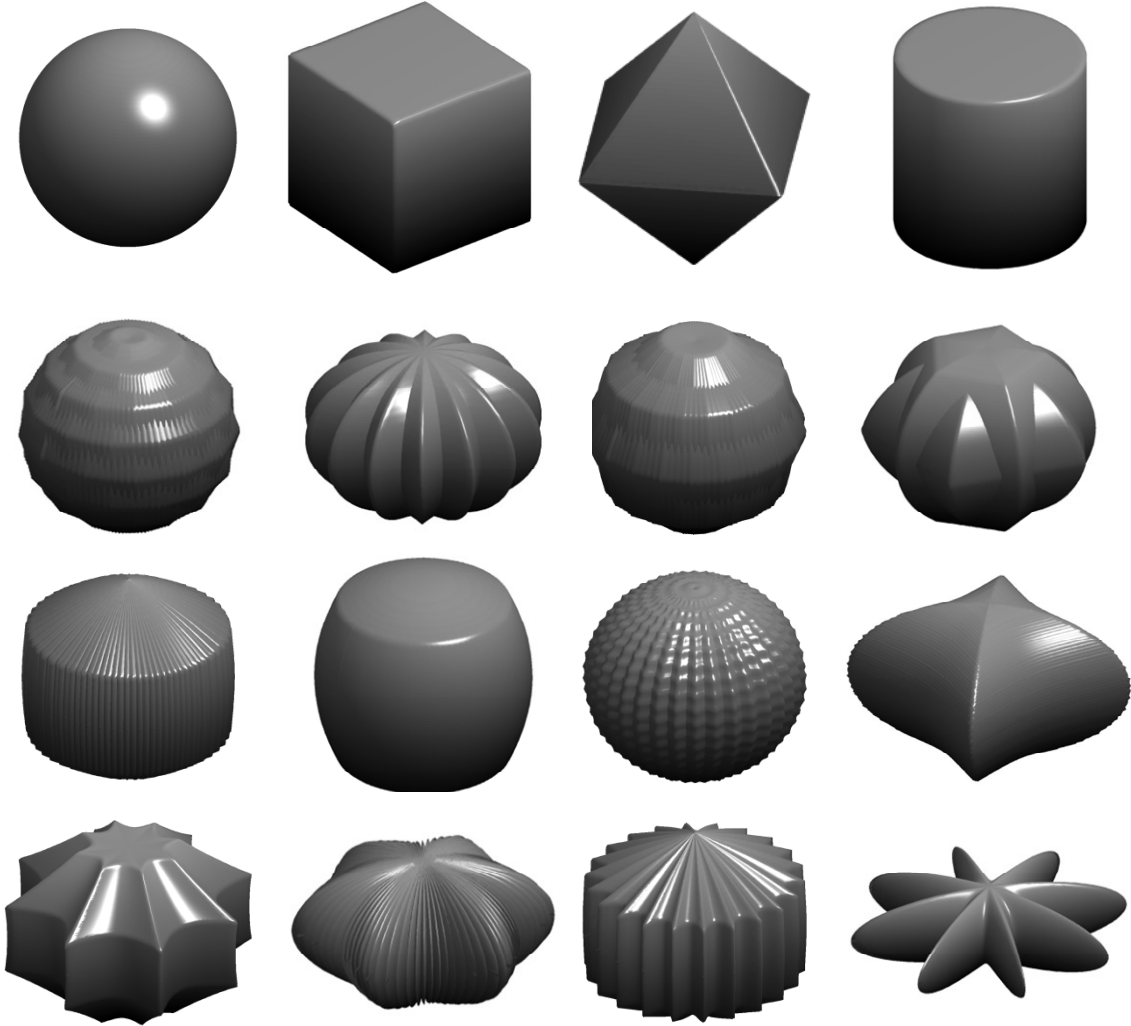


Figure 2. A class of shapes defined by the 3D Gielis' superformula.

Since a larger short circuit current density  $J_{sc}$  indicates a higher open circuit voltage and higher conversion efficiency for solar cells, thus  $J_{sc}$  is selected as the cost function to be maximized in the optimization. If each electron-hole pair contributes to the photocurrent, namely 100% internal quantum efficiency,  $J_{sc}$  is defined as

$$J_{sc} = e \int \lambda / (hc) QE(\lambda) I_{AM1.5}(\lambda) d\lambda \quad (2)$$

where  $e$  denotes the charge on an electron,  $h$  the Plank's constant,  $\lambda$  wavelength and  $c$  the speed of light in vacuum. The quantum efficiency  $QE(\lambda) = P_{abs}(\lambda) / P_{in}(\lambda)$  is the ratio of the power of the absorbed light  $P_{abs}(\lambda)$  to that of the incident light  $P_{in}(\lambda)$  within the Si film.  $I_{AM1.5}$  stands for the relevant part of the solar spectral irradiance. Once Maxwell's system is solved, the short circuit current density ( $J_{sc}$ ), electric intensity, absorption as well as other

relevant factors can be computed to any pre-defined level of accuracy. In the simulation, 300 equally spaced frequency points are considered in the solar spectrum between  $\lambda=300\text{nm}$  and  $\lambda=840\text{nm}$ .

Shape optimization for nanoparticles is aimed to search for a stationary point in the hyperspace defined by parameters  $(m, n_1, n_2, q, n_4, n_5)$  so that an extremal value of the cost function is achieved. Considering that the number of parameters to be determined is relatively small, we adopt the evolutionary algorithm [13] for the optimization. Such a non-gradient method is fairly simple but efficient, especially suitable for optical optimization in which the gradient of the cost function with respect to the design variables is often too sensitive to be controlled and stabilized in terms of other and our previous studies in [14, 15]. The evolutionary algorithm starts from a set of parent vectors randomly selected in the given parametric space. For each parent vector, a fitness (to be maximized) is obtained by solving Maxwell's equations. Then an offspring is introduced by a certain mutation rule that is defined as the summation of the weighted difference between a pair of parent vectors and the third. The offspring is required to mend by a cross-over process for improving the diversity. In this step the weighing factor and cross-over probability are set to be 0.5 and 1, respectively, for the following examples. The mutation and cross-over processes are repeated until the best performance is obtained. The upper and lower bounds of the design variables must be determined before the optimization and they should be wide enough to encompass the feasible values. Through a number of tests, we determined that the bounds for  $m$  and  $q$  are the same, ranging from 2 to 180 and the ranges for shape parameters  $n_1, n_2, n_4$  and  $n_5$  are from 0.001 to 20000.

To balance the size effect on the surface resonance, all candidate structures are weighted by a factor so that the maximal spatial span in  $x$  or  $y$  direction is 200 nm. In the computational model, the space containing the nanoparticle is discretized in  $40 \times 40 \times 40$  cubic mesh (i.e. 5 nm mesh size) for the FDTD solution to Maxwell's equations. Finer mesh size (3 nm, around  $66 \times 66 \times 66$  elements) is employed for the optimal and alternative geometries in order to generate more distinct electric field distribution. It is found that around 0.15% increase in  $J_{sc}$  is obtained when using the 3 nm mesh. Such a slight change indicates that the 5 nm mesh is fine enough to properly describe the geometrical features and electromagnetic responses of the nanoparticle. Out of a wide variety of sophisticated 3D geometries defined by the Gieles' superformula, the optimization process yields a lens-like structure (Figure 3a-b) that makes the thin-film solar cell have a  $J_{sc}$  approaching to  $19.11 \text{ mA/cm}^2$ , 3.3% higher than the benchmarking value ( $J_{sc} = 18.50 \text{ mA/cm}^2$ ) of the two-scale nanospheres shown in Figure 1b.

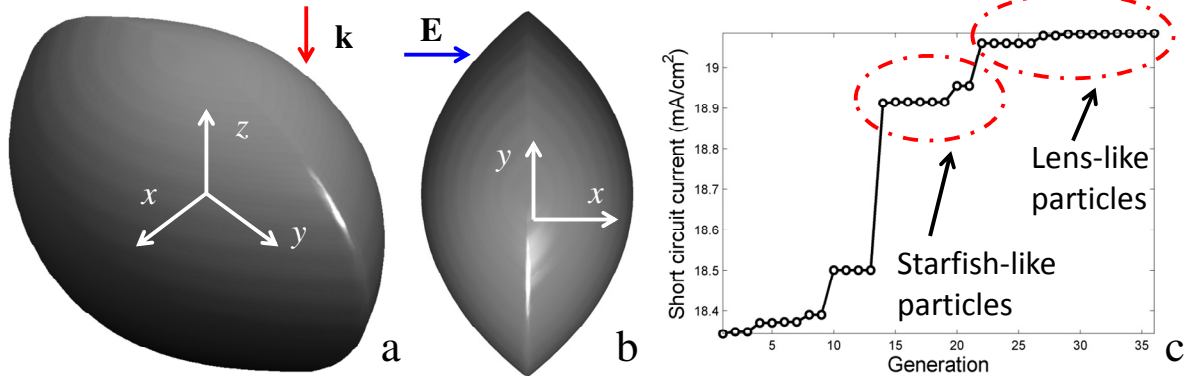


Figure 3. (a) Perspective and (b) top views of the optimized lens-like particle; (c) The convergence history of the cost function during the optimization process.

The convergence history of the cost function ( $J_{sc}$ ) with respect to the iteration step (generation) is plotted in Figure 3c, indicating that the cost function almost reaches the peak at the 22<sup>nd</sup> generation and then slightly increases in subsequent steps. The nanoparticles corresponding to these steps are very similar as shown in Figure 4 which illustrates the contours of the central cross sections in the horizontal (Figure 4a) and vertical (Figure 4b) symmetry planes. Figure 4 also indicates that  $J_{sc}$  remains at a high value between  $19.03$  and  $19.11 \text{ mA/cm}^2$  even though the shape variation of these lens-like structures is notable. Such a robust performance is of critical importance to mass-production as certain fabrication errors, usually unavoidable in nanoscale, can be tolerated by this novel structure. Moreover, compared with the two-scale nanosphere, the lens-like structure is far easier to be fabricated due to its much simpler geometry.

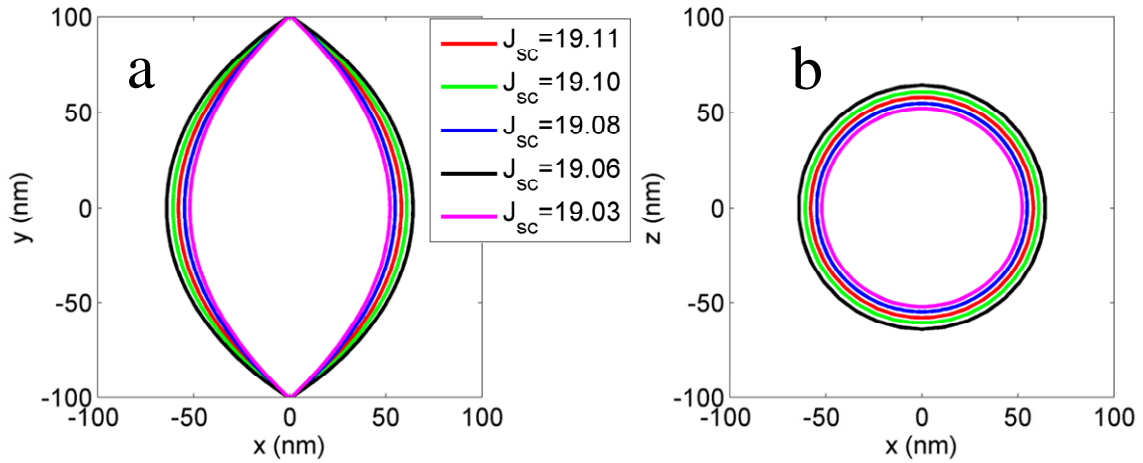


Figure 4. The attained  $J_{sc}$  and cross sectional profiles of the lens-like particle in (a) horizontal symmetry plane; (b) vertical symmetry plane.

The Gielis' parameters for this optimal lens-like structure are  $m=2$ ,  $n_1=780.615$ ,  $n_2=1239.8594$ ,  $q=180$ ,  $n_4=19535.7177$  and  $n_5=230.1503$ , which result in 5.18% nanoparticle coverage for the thin-film solar cell. As the coverage is much smaller than the widely-accepted optimal coverage (10%) [1, 7] with randomly-shaped nanoparticles, the cost can be significantly reduced because less silver material is required. On the other hand, the volume ratio of this novel structure to the benchmark two-scale sphere is around 30%, indicating that the increase in  $J_{sc}$  is attributed to the shape as a larger volume will induce stronger surface plasmon and therefore result in a larger  $J_{sc}$ . Additional evidence supporting the proposition that the improved performance is due to the shape, rather than the volume is that the optimal nanoparticle (red contour in Figure 4) with the maximal  $J_{sc}$  has an intermediate volume compared with its counterparts described by the shape profiles in different colors.

A near-field optical contour can be plotted to explain the enhancement of the short circuit current density. Figures 5a-b illustrate the near-field electric intensity ( $|\mathbf{E}|^2$ ) on vertical and horizontal symmetry planes, respectively, at the time when  $|\mathbf{E}|^2$  reaches the maximum on the horizontal symmetry plane. It is seen that the near-field intensity is evidently strengthened in the bilateral vertices (Figure 5b) and the bottom part (Figure 5a) around the nanoparticle. Note that the upper Si film then takes advantage of such a light concentration to enhance its absorption. Since the normal directions of the nanoparticle surface are not vertical, the resonant electromagnetic wave impinges upon the rear metal and subsequently is reflected into the absorbing Si layer at large angles. As a result, the effective light path is prolonged. The snapshot in Figure 5c presents the contour of the relative absorption per unit volume ( $A = \log_{10}[\text{Im}(\epsilon)|\mathbf{E}|^2]$ ) in different layers of the solar cell on the vertical symmetry plane. It shows that the reflection from the rear Ag layer, together with the scattering and diffraction caused by the nanostructural geometry, results in strong absorption in the Si film. Because the gap between the nanoparticle and Si layer is relatively small (20 nm), the near-field of the surface plasmon resonance is capable of coupling into the lower part of the Si film, thereby improving the absorption in this region. The gradient direction of absorption (as arrowed in Figure 5c) clearly indicates that the energy flux interacts with the rear Ag layer at large angles and traps the light within the Si film.

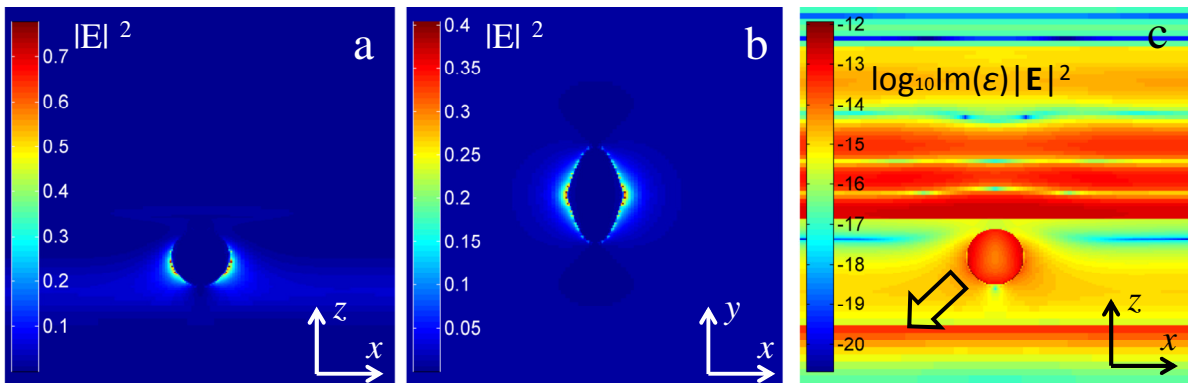
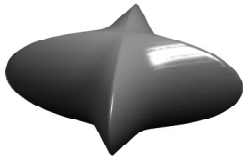
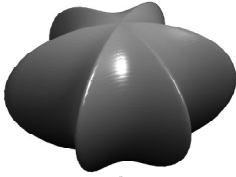
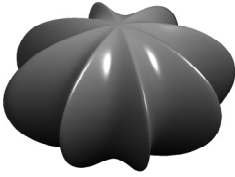

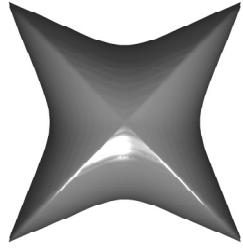
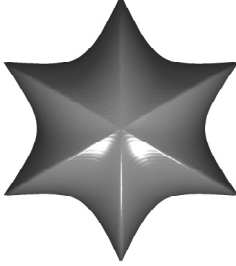

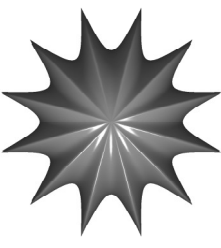


Figure 5. The electric intensity on the cross section of optimal lens-like nanoparticle in (a) vertical symmetry

plane; (b) horizontal symmetry plane; (c) Distribution of relative absorption per unit volume on the vertical symmetry plane.

In addition to lens-like structure, the optimization process has also resulted in a series of starfish-like nanoparticles with different number of arms (as shown in Table 1), which allow attaining relatively large short circuit current density. It is found that the starfish-like nanoparticles with 4, 6 and 8 arms have fairly similar circuit current density ( $J_{sc} \approx 19.02 \text{ mA/cm}^2$ ) even though their shapes are notably different. Interestingly, such shapes are generated from the intersection of even number (e.g.  $m=4, 6$  and  $8$ ) of lens-like structures with rotational symmetry. The small disparity in the attained  $J_{sc}$  is because the lens-like nanoparticle is not strictly symmetric, rendering that the distance to neighboring nanoparticles along the  $x$  and  $y$  directions slightly differs and therefore influences the coupling effect between them. The geometric parameters and the coverage of these starfish-like nanostructures are summarized in Table 1. Note that the coverage of these nanoparticles devised for the thin-film solar cells is smaller than the “optimal” 10% value.

Table 1: Starfish-like nanoparticles for thin-film solar cells

	starfish with 4 arms	starfish with 6 arms	starfish with 8 arms	starfish with 12 arms
3D View				
Top View				
$J_{sc}$	19.0270	19.0133	19.0270	18.9385
$m$	4	6	8	12
$n_1$	622.9241	1037.0787	1243.55	1072.7683
$n_2$	1427.3839	1440.5443	1829.2571	1529.5176
$q$	172	146	90	120
$n_4$	19979.1638	9074.9848	16808.8015	19700.8845
$n_5$	170.4596	95.0665	28.3528	28.6072
Coverage	8.03%	5.87%	6.60%	6.24%

A glimpse into the electric field intensity of the starfish-like nanoparticles is shown in Figures 6a-b for the horizontal and vertical symmetry planes, respectively. The surface plasmon can be clearly observed around the sharp vertices (Figures 6a-c), which is believed to be a complementary way for such field-enhanced ‘antennas’ [16]. The scattered light is amplified in the dielectric ZnO layer adjacent to the bilateral sides of the bottom part of the nanoparticles. The area of field-enhanced region is almost similar to the nanoparticle size and is far away from the nanoparticle, reflecting that the Ohmic loss on the nanoparticle surface can be reduced. The gradient direction (indicated by white arrows in Figures 6d-f) of the electric field intensity in vertical symmetry plane illustrates that the nanoparticles render large scattering angles.



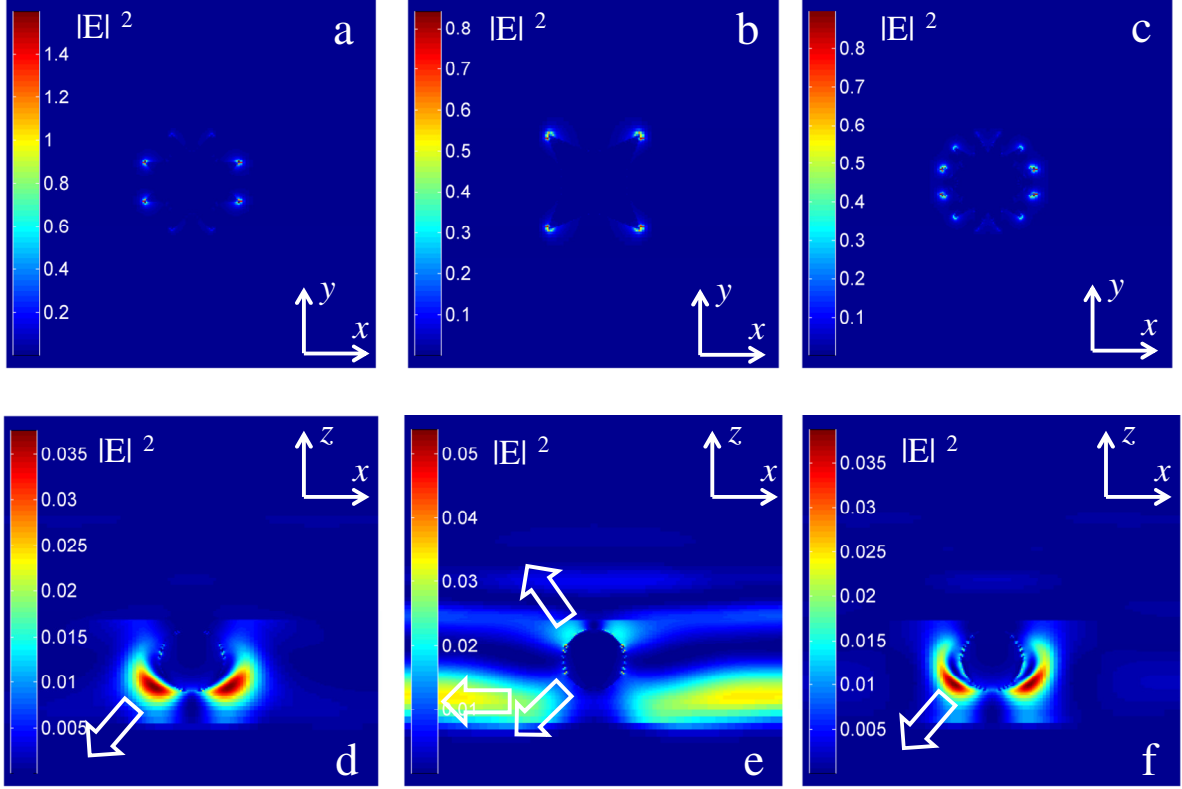


Figure 6. The electric field intensity on horizontal/vertical symmetric planes for starfish-like nanoparticles with (a/d) 8 arms; (b/e) 4 arms; (c/f) 12 arms.

Interestingly, similar shapes to the cross sectional geometry of these starfish-like structures (e.g. top view of the starfish-like structures with four and six arms) have been reported elsewhere by Macías *et al.* [10] recently when they attempted to search for 2D shapes with maximal scattering cross section. It is not surprising that their 2D counterparts have a similar electric field intensity distribution (Figures 6a-b). Nevertheless, it is found that  $J_{sc}$  decreases when the starfish-like nanoparticle has too many vertices (e.g. the one with 12 arms in Table I only results in  $J_{sc} = 18.93 \text{ mA/cm}^2$ ), possibly owing to a strong resonant interaction between these multiple arms which induces a large Ohmic loss for the nanoparticle. In the meantime, the novel nanoparticles can couple sunlight into the surface plasmon polariton mode (a bounded horizontal wave in the ZnO film as shown by the white arrow in Figure 6e), indicating another effective way for trapping and guiding light in the Si film. In this mode, the solar flux is turned by  $90^\circ$ , allowing for a much longer lighting path within the Si film.

The number of absorbed photons in the Si film is proportional to  $J_{sc}$ , thus its change across the sunlight spectra can be used to further explore the role of nanoparticles. Since the sunlight with short wavelength ( $\lambda < 550 \text{ nm}$ ) is reflected or absorbed before reaching the ZnO layer where nanoparticles are embedded, the numbers of absorbed photons (as shown in Figure 7) in these three solar cells considered, i.e. (1) two-scale spherical nanoparticles (blue curve dotted with + markers), (2) optimal lens-like nanoparticles (black curve) and (3) the 8-armed starfish-like nanoparticles (red dashed curve) are nearly the same. Compared with the photons in natural sunlight (green dashed-dot curve), the absorbed photons account for a substantial fraction of the total energy. In the range of  $550\text{-}770 \text{ nm}$  (except for a few narrow ranges), the two-scale spherical particle exhibits a certain advantages over our designs, possibly because the small spheres are able to scatter sunlight into larger angles in this range [7] while the volume of the large sphere is three times greater than ours. In the red light range ( $770 < \lambda < 840 \text{ nm}$ ) where the scattering effect of small spheres decay, the number of absorbed photons falls sharply. However, our new nanoparticles show some amazing scattering effects in this range and make their performance over the whole sunlight spectra exceed that of the two-scale nanospheres.

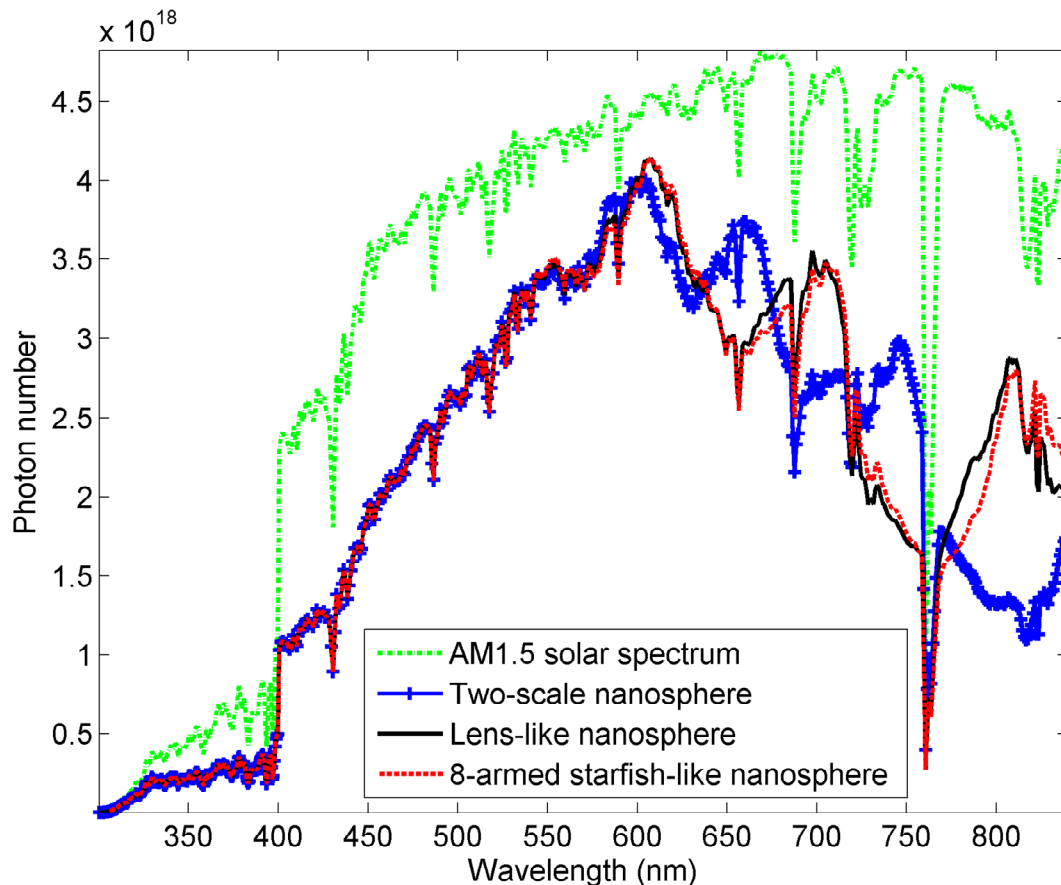


Figure 7. The number of photons in natural sunlight and absorbed in the Si film with different designs of nanoparticles across the sunlight spectrum.

The ongoing studies on thin-film solar cells have already demonstrated that the noble metal nanoparticles embedded into the rear dielectric layer can enhance the short circuit current densities and provide unique capability of generating localized surface plasmon and changing scattering angles. This work systemically explored the relationship between a variety of sophisticated shapes defined by the 3D Gielis' superformula and  $J_{sc}$ . We have found two types of novel geometries, namely lens-like and starfish-like nanoparticles, which allow generating larger  $J_{sc}$  than the two-scale nanospheres that were devised previously.

It is important to note that the novel nanoparticles are fabrication-friendly due to their simpler shapes and insensitivity to geometric variations. Our numerical simulations have demonstrated that these novel nanoparticles can yield strong local field enhancement, large scattering angle and high surface plasmon polariton, which are accepted as the only three effective ways to enhance the absorption in the Si film for thin-film solar cells [1]. The methodology presented in this paper has potential to be applied to the design of other shape-related electromagnetic devices such as nanoantennas [17], biological/chemical nano-sensors [16], and plasmonic lenses [15].

## 5. Acknowledgements

This work was supported by an Australian Research Council Discovery Early Career Researcher Award (project number DE120102906) and an Australian Research Council Discovery Project grant (DP110104698).

## 6. References

1. H. A. Atwater and A. Polman, Plasmonics for improved photovoltaic devices, *Nature Materials*, 9, 205–213 2010.
2. M. A. Green, *Solar Cells: Operating Principles, Technology and System Applications* The University of New South Wales, Sydney, 1998.
3. F. J. Beck, A. Polman, and K. R. Catchpole, Tunable light trapping for solar cells using localized surface plasmons, *Journal of Applied Physics*, 105, 114310 2009.
4. K. R. Catchpole and A. Polman, Design principles for particle plasmon enhanced solar cells, *Applied Physics*



- Letters*, 93, 191113 2008.
5. S. Pillai, K. R. Catchpole, T. Trupke, and M. A. Green, Surface plasmon enhanced silicon solar cells *Journal of Applied Physics*, 101, 093105 2007.
  6. Z. Ouyang, S. Pillai, F. Beck, O. Kunz, S. Varlamov, K. R. Catchpole, P. Campbell, and M. A. Green, Effective light trapping in polycrystalline silicon thin-film solar cells by means of rear localized surface plasmons, *Applied Physics Letters*, 962010.
  7. X. Chen, B. H. Jia, J. K. Saha, B. Y. Cai, N. Stokes, Q. Qiao, Y. Q. Wang, Z. R. Shi, and M. Gu, Broadband enhancement in thin-film amorphous silicon solar cell enabled by nucleated silver nanoparticles, *Nano Letters*, 12, 2187–2192 2012.
  8. J. Gielis, A generic geometric transformation that unifies a wide range of natural and abstract shapes, *American Journal of Botany*, 90, 333–338 2003.
  9. J. T. B. Overvelde, S. Shan, and K. Bertoldi, Compaction through buckling in 2D periodic, soft and porous structures: effect of pore shape, *Advanced Materials*, 24, 2337-2242 2012.
  10. D. Macías, P. M. Adam, V. Ruíz-Cortés, R. Rodríguez-Oliveros, and J. A. Sánchez-Gil, Heuristic optimization for the design of plasmonic nanowires with specific resonant and scattering properties, *Optics Express*, 20, 13146-13163 2012.
  11. K. Yee, Numerical solution of initial boundary value problems involving Maxwell's equations in isotropic media, *IEEE Transactions on Antennas and Propagation*, 14, 302–307 1966.
  12. <http://www.lumerical.com> (Access on Dec.1 2012).
  13. R. Storn and K. Price, Differential Evolution – A Simple and Efficient Heuristic for Global Optimization over Continuous Spaces, *Journal of Global Optimization*, 11, 341–359 1997.
  14. S. W. Zhou, W. Li, Y. H. Chen, G. Y. Sun, and Q. Li, Topology optimization for negative permeability metamaterials using level-set algorithm, *Acta Materialia*, 59, 2624-2636 2011.
  15. S. W. Zhou, W. Li, G. Y. Sun, and Q. Li, A level-set procedure for the design of electromagnetic metamaterials, *Opt Express*, 18, 6693-6702 2010.
  16. A. García-Etxarri, P. Apell, M. Käll, and J. Aizpurua, A combination of concave/convex surfaces for field-enhancement optimization: the indented nanocone, *Optics Express*, 20, 25201-25212 2012.
  17. P. Mühlischlegel, H. J. Eisler, O. J. F. Martin, B. Hecht, and D. W. Pohl, Resonant optical antennas, *Science* 308, 1607-1609 2005.